

NASA/TM–2017-219673



UAV Inspection of Electrical Transmission
Infrastructure with Path Conformance Autonomy
and Lidar-based Geofences
NASA Report on UTM Reference Mission Flights at
Southern Company Flights November 2016

Andrew J. Moore
Langley Research Center, Hampton, Virginia

Matthew Schubert
Analytical Mechanics Associates, Inc., Hampton, Virginia

Nicholas Rymer and Swee Balachandran
National Institute of Aerospace, Hampton, Virginia

Maria Consiglio and Cesar Munoz
Langley Research Center, Hampton, Virginia

Joshua Smith
University of Arkansas, Fayetteville, Arkansas

Dexter Lewis
Southern Company Services, Birmingham, Alabama

Paul Schneider
Georgia Power, Atlanta, Georgia

October 2017

NASA STI Program . . . in Profile

Since its founding, NASA has been dedicated to the advancement of aeronautics and space science. The NASA scientific and technical information (STI) program plays a key part in helping NASA maintain this important role.

The NASA STI program operates under the auspices of the Agency Chief Information Officer. It collects, organizes, provides for archiving, and disseminates NASA's STI. The NASA STI program provides access to the NTRS Registered and its public interface, the NASA Technical Reports Server, thus providing one of the largest collections of aeronautical and space science STI in the world. Results are published in both non-NASA channels and by NASA in the NASA STI Report Series, which includes the following report types:

- **TECHNICAL PUBLICATION.** Reports of completed research or a major significant phase of research that present the results of NASA Programs and include extensive data or theoretical analysis. Includes compilations of significant scientific and technical data and information deemed to be of continuing reference value. NASA counter-part of peer-reviewed formal professional papers but has less stringent limitations on manuscript length and extent of graphic presentations.
- **TECHNICAL MEMORANDUM.** Scientific and technical findings that are preliminary or of specialized interest, e.g., quick release reports, working papers, and bibliographies that contain minimal annotation. Does not contain extensive analysis.
- **CONTRACTOR REPORT.** Scientific and technical findings by NASA-sponsored contractors and grantees.

- **CONFERENCE PUBLICATION.** Collected papers from scientific and technical conferences, symposia, seminars, or other meetings sponsored or co-sponsored by NASA.
- **SPECIAL PUBLICATION.** Scientific, technical, or historical information from NASA programs, projects, and missions, often concerned with subjects having substantial public interest.
- **TECHNICAL TRANSLATION.** English-language translations of foreign scientific and technical material pertinent to NASA's mission.

Specialized services also include organizing and publishing research results, distributing specialized research announcements and feeds, providing information desk and personal search support, and enabling data exchange services.

For more information about the NASA STI program, see the following:

- Access the NASA STI program home page at <http://www.sti.nasa.gov>
- E-mail your question to help@sti.nasa.gov
- Phone the NASA STI Information Desk at 757-864-9658
- Write to:
NASA STI Information Desk
Mail Stop 148
NASA Langley Research Center
Hampton, VA 23681-2199

NASA/TM-2017-219673



UAV Inspection of Electrical Transmission Infrastructure with Path Conformance Autonomy and Lidar-based Geofences NASA Report on UTM Reference Mission Flights at Southern Company Flights November 2016

Andrew J. Moore
Langley Research Center, Hampton, Virginia

Matthew Schubert
Analytical Mechanics Associates, Inc., Hampton, Virginia

Nicholas Rymer and Swee Balachandran
National Institute of Aerospace, Hampton, Virginia

Maria Consiglio and Cesar Munoz
Langley Research Center, Hampton, Virginia

Joshua Smith
University of Arkansas, Fayetteville, Arkansas

Dexter Lewis
Southern Company Services, Birmingham, Alabama

Paul Schneider
Georgia Power, Atlanta, Georgia

National Aeronautics and
Space Administration

Langley Research Center
Hampton, Virginia 23681-2199

October 2017

Acknowledgments

We are grateful to the many NASA Langley colleagues for early discussions about the various facets of this mission: Tom Vranas (UAV platform design and testing), Scott Dorsey (ultraviolet sensing), Taumi Daniels (corona physics), Kelly Hayhurst and Jill Brown (mission and regulatory framework), George Hagen (ICAROUS capacity test), and Evan Dill and Robert McSwain (differential GPS). Leo Wang and Daniel Mulfinger of the NASA Ames UTM group assisted with airspace tracking technology. James Hubbard of the National Institute of Aerospace and the University of Maryland provided advice about the mission. J. Smith acknowledges the University Space Research Association for internship logistics. This work was performed with support from the NASA Safe Autonomous Systems Operations program, under the direction of Sharon Graves.

The use of trademarks or names of manufacturers in this report is for accurate reporting and does not constitute an official endorsement, either expressed or implied, of such products or manufacturers by the National Aeronautics and Space Administration.

Available from:

NASA STI Program / Mail Stop 148
NASA Langley Research Center
Hampton, VA 23681-2199
Fax: 757-864-6500

Abstract

Flights at low altitudes in close proximity to electrical transmission infrastructure present serious navigational challenges: GPS and radio communication quality is variable and yet tight position control is needed to measure defects while avoiding collisions with ground structures. To advance unmanned aerial vehicle (UAV) navigation technology while accomplishing a task with economic and societal benefit, a high voltage electrical infrastructure inspection reference mission was designed. An integrated air-ground platform was developed for this mission and tested in two days of experimental flights to determine whether navigational augmentation was needed to successfully conduct a controlled inspection experiment. The airborne component of the platform was a multirotor UAV built from commercial off-the-shelf hardware and software, and the ground component was a commercial laptop running open source software. A compact ultraviolet sensor mounted on the UAV can locate “hot spots” (potential failure points in the electric grid), so long as the UAV flight path adequately samples the airspace near the power grid structures. To improve navigation, the platform was supplemented with two navigation technologies: lidar-to-polyhedron preflight processing for obstacle demarcation and inspection distance planning, and trajectory management software to enforce inspection standoff distance. Both navigation technologies were essential to obtaining useful results from the hot spot sensor in this obstacle-rich, low-altitude airspace. Because the electrical grid extends into crowded airspaces, the UAV position was tracked with NASA unmanned aerial system traffic management (UTM) technology. The following results were obtained:

- Inspection of high-voltage electrical transmission infrastructure to locate “hot spots” of ultraviolet emission requires navigation methods that are not broadly available and are not needed at higher altitude flights above ground structures.
- The sensing capability of a novel airborne UV detector was verified with a standard ground-based instrument. Flights with this sensor showed that UAV measurement operations and recording methods are viable. With improved sensor range, UAVs equipped with compact UV sensors could serve as the detection elements in a self-diagnosing power grid.
- Simplification of rich lidar maps to polyhedral obstacle maps reduces data volume by orders of magnitude, so that computation with the resultant maps in real time is possible. This enables real-time obstacle avoidance autonomy. Stable navigation may be feasible in the GPS-deprived environment near transmission lines by a UAV that senses ground structures and compares them to these simplified maps.
- A new, formally verified path conformance software system that runs onboard a UAV was demonstrated in flight for the first time. It successfully maneuvered the aircraft after a sudden lateral perturbation that models a gust of wind, and processed lidar-derived polyhedral obstacle maps in real time.
- Tracking of the UAV in the national airspace using the NASA UTM technology was a key safety component of this reference mission, since the flights were conducted beneath the landing approach to a heavily used runway. Comparison to autopilot tracking showed that UTM tracking accurately records the UAV position throughout the flight path.

Introduction

Is current UAV navigational technology sufficient to inspect essential infrastructure? At altitudes above trees and buildings, waypoint-based autonomy via GPS guidance available in commercial autopilots is sufficient. However, at lower altitudes in close proximity to structures,

GPS and radio communication quality is variable, and yet position control within a narrow tolerance is needed to measure defects while avoiding collisions with ground structures. This report describes the navigational impact of radio degradation in one example of an obstacle-rich low-altitude airspace – air corridors adjacent to high-voltage transmission structures – and tests techniques to ensure safe, effective UAV traversal in those airspaces.

Report Overview and Findings

To provide realistic operational constraints and to bound the range of acceptable results, a specific mission was designed that requires UAV flight paths which sample the airspace near ground structures: inspection of high-voltage electrical transmission infrastructure to locate “hot spots” of ultraviolet emission. Flights with an airborne UV sensor near two test hot spot locations on a 500 kV structure are described. Comparison of the signals detected at points along the flight path to readings from a standard UV camera shows that UAV-based corona detection in real time is a viable alternative to ground-based detection.

Transient perturbations of aircraft position due to wind gusts add to the control challenge posed by radio degradation in this mission environment. Tests of a novel onboard flight path conformance software system are described for flights with and without a perturbation that models wind gusts. The system successfully maneuvered the UAV back onto the preplanned flight path after the perturbation, and did not alter the UAV path in the unperturbed flight.

The intermittency of GPS in this mission environment can be ameliorated by taking advantage of rich lidar maps of transmission infrastructure routinely collected by electric utilities. The richness of this data creates a computation challenge; unless simplified, the data volume of the raw lidar maps is too high for real time processing. Two methods of simplification are described that reduce data volume by orders of magnitude. Both methods are evaluated as aids for mission planning and for interpretation of UV sensor readings to find hot spots. The computational fitness of the simplified maps as navigational tools is analyzed, and it is concluded that the data volume reduction enables their use for rotary UAV navigation in a dense obstacle field.

Because the electrical transmission grid extends into crowded airspaces, the UAV position was tracked with UTM technology. For all flights, UTM tracking results are presented side by side with groundstation autopilot tracking. While UTM time sampling is lower than autopilot tracking, the UTM flight path records were found to be adequate to represent the results.

Significance of the Reference Task

Airborne avionics to sense transmission line faults and onboard computing to safely guide a UAV near high-voltage structures are essential components of an autonomous UAV-based electrical grid inspection capability. A fleet of UAVs equipped with these components could autonomously examine high-voltage structures, pinpointing locations of the grid with damage and equipment malfunction that represent potential or actual risks to power delivery. If distributed across a power grid (for example, at substations), this fleet could serve as the detection foundation of a self-diagnosing power grid (Figure 1). Imagery and other telemetry from the UAV deployments could then be interpreted remotely by experienced grid operation crews and line crews, enabling the rapid dispatch of a nearby line crew in a repair truck loaded with the components necessary to repair the fault. Given the economic and societal benefit of this concept and its need for advanced aeronautical technology, high voltage electrical infrastructure inspection with a rotary UAV was selected as a reference mission to pursue within NASA’s Unmanned Aerial System Traffic Management (UTM) program.

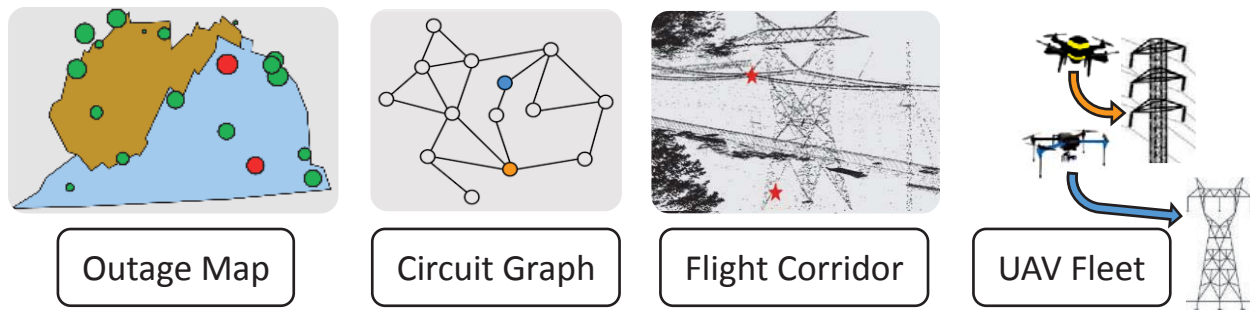


Figure 1. Components of a self-diagnosing power grid. UAVs cached at locations across the grid, such as electrical substations, can be deployed on demand to locate and characterize the faults based on geographic outage maps and topological circuit maps. ©Lidar data: Southern Company

Flight Test Technologies and Related Literature

Tracking such a fleet in the national airspace is needed to ensure that the operation of each UAV takes into account other members of the fleet, other UAVs, and manned aircraft [3]. At altitudes above buildings and vegetation, geolocation via onboard GPS is reliable enough and accurate enough to prevent collision with other vehicles using self-separation and alerting technology [4]. At the low altitudes of transmission lines, however, the complexity of measures required for safe flight increases, since precise geolocation of nearby obstacle fields and navigational means to avoid them is needed [12].

Safe operations of small UAS vehicles in uncontrolled airspace is a major goal of NASA's Unmanned Aerial System (UAS) Traffic Management (UTM) project [3]. A far-term aim of UTM research and development is to accommodate small UAS operations throughout the National Airspace System at low altitudes for beyond visual line-of-sight operations.

This study demonstrates an integrated air-ground UAV flight platform performing an electrical transmission line inspection reference mission at low altitudes in a densely occupied flight field. The UAV was built from commercial equipment and software supplemented with the following NASA-developed technologies:

- lidar-to-polyhedron preflight processing for obstacle demarcation to determine inspection standoff distance;
- ICAROUS¹ [5, 6] flight path conformance software to monitor inspection standoff distance and correct the UAV trajectory during autonomous waypoint-based flight;
- telemetry repeater software to send the UAV position to a NASA UTM air traffic management server for tracking in the national airspace; and,
- compact airborne ultraviolet (UV) sensing to detect transmission line faults.

In this report, eleven fully instrumented line-of-sight flights are described at altitudes up to 18 meters (59 feet) above ground level. For all flights, trajectory data from the autopilot and from the UTM server are compared with a lidar-derived polygonal geofence. For two of the flights, the difference between the actual and planned trajectory is also compared, so as to illuminate the operation of the ICAROUS flight path conformance autonomy.

¹ Integrated Configurable Algorithms for Reliable Operations of Unmanned Systems

High fidelity aerial lidar data of the test site was converted to polyhedral obstacle maps using both a 2.5D method and a 3D method². The data reduction afforded by the two methods is compared and the processing capacity of the ICAROUS software on the specific hardware used in the flights is examined with reference to these polyhedral obstacle maps.

Sensors and concepts for autonomous transmission line inspection are reviewed in [1, 2]. A review of compact corona detection for transmission line inspection is provided in [8]. Data reduction approaches for 3D lidar point clouds are reviewed in [9]. Airborne lidar (also known as airborne laser scanning) was adopted broadly by the utility industry in the last decade to meet transmission line safety requirements [18].

Test and Measurement Flights

Flight Locations, Objectives, and Datatypes

All flights described in this report were conducted at Southern Company's Klondike training facility in Lithonia, Georgia, on November 15 and 16, 2016, with a NASA-built UAV. The flight locations and ground camera positions (Figure 2) were adjacent to a de-energized structure rated for 500kV electric power transmission (steel lattice tower with insulators and associated conductors). Video and corona camera tripods were placed 60 to 90 meters from the flight locations to accommodate the small depth of field of the corona camera. The site is 17.5 miles due east of the bustling Hartsfield–Jackson Atlanta International Airport (KATL), beneath a landing approach corridor. Throughout these flights, aircraft on descent approach to KATL flew 5000 feet overhead [25] at a rate of about once per minute

Table 1 lists the conditions and data types for each of the three sets of flights that are described in this report. Lower altitude (corona measurement flights ('B flights')) took place at the base of the steel lattice tower on the afternoon of first day; higher altitude corona measurement flights ('T flights') took place at the point of conductor attachment to the tower on the end of the first day. A corona generator was attached to the structure for the B and T flights, and the corona intensity detected at the UAV position by a pair of onboard compact ultraviolet sensors was transmitted in real time to a ground station laptop, as indicated by a check in the 'UV plot' column of Table 1. 'UV Image' and 'Visible Image' columns in Table 1 indicate recording with the ground-based corona camera and visible camera. The corona generator intensity was adjusted to ensure detection at a standoff distance of six meters (twenty feet; this intensity is higher than created by a 100 kV corona; see [8] for details and a discussion of the options to increase sensor range).

Telemetry repeater software on the ground station laptop forwarded the UAV's position to a NASA air traffic management server for tracking in the national airspace in the final two T flights. This position information is referred to as the UTM (UAS Traffic Management system) Path in Table 1. The UTM Path and UTM Boundary datatypes were collected during a set of autonomous trajectory correction flights ('I flights'), which took place on the afternoon of the second day.

² Terrestrial maps may ignore altitude, for example, by projecting all elevations to ground. This is a two-dimensional (2D) map. A map with altitude represented by a single value, such as the height of a rooftop, is known as a topographic or 2.5D map. A 2.5D map, while compact, cannot depict features such as tunnels, overhangs on buildings, and open areas under tree canopies. To represent such features a full 3D map is needed.

Flights are designated according to the set, day, and flight count³: lower altitude (up to 5 meters) corona flights, all executed on the first day, are designated as B1_1 and B1_2; tower flights are designated as T1_2, T1_3, T2_2 and T2_3; trajectory correction flights are designated as I2_1 and I2_3. A full inventory of flights is provided in Appendix 1⁴. Appendix 2 documents all equipment and software used in these flights.

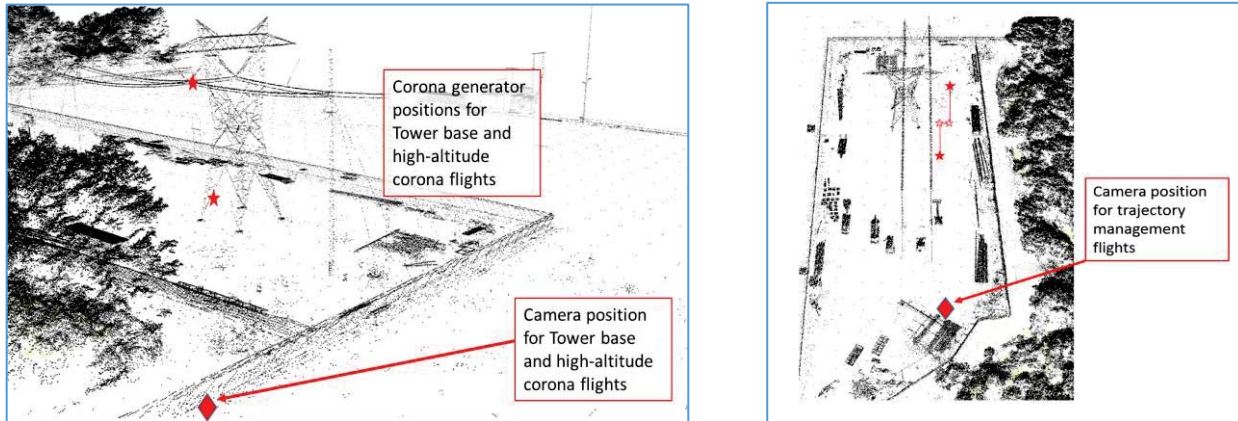


Figure 2. Flight locations (stars) and camera positions (red diamonds) at Southern Company's Klondike training facility in Lithonia, Georgia. ©Lidar data: Southern Company

Tower base corona measurement flights ('B flights')

In the first flight series the corona generator was magnetically attached to the base of the steel lattice tower. A manual flight (B1_1) successfully tested the UAV, the radio controller (RC transmitter), ground station control and telemetry, and the compact UV sensor. The three peaks in the UV signal plot (Table 2, row B1_1) correspond to manually executed traversals of the UAV in front of the generator; since the UAV was oriented with its nose pointed west, only the right sensor faced the generator. (See Figure 3 for sensor placement and the B1_1 flight path image of Table 2 for compass and UAV orientations.) Using altitudes and waypoints ascertained from this flight, an autonomous flight

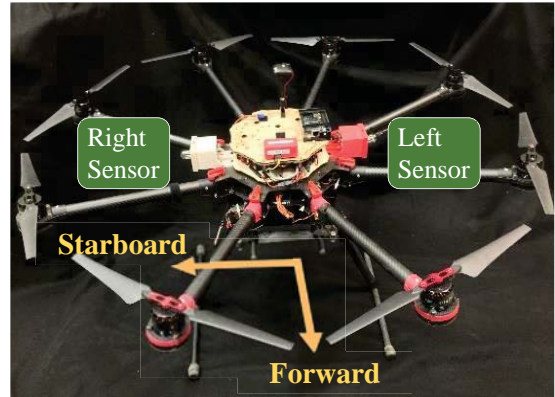


Figure 3. Compact UV sensor orientation

³ BD_R (B=Base of tower, D=Day, R=Repetition), TD_R (T=Top of tower, D=Day, R=Repetition), ID_R (I=ICAROUS, D=Day, R=Repetition)

⁴ Some flights included in full inventory in Appendix 1 are not described at length in the body of this report (T1_1, T2_1, and I2_1). An incorrect geofence ceiling of 20 meters prevented climbing to a useful height during Flight T1_1. An incorrect waypoint or a GPS fault caused the UAV to fly off the intended flight path at the start of flight T2_1, so the flight was aborted quickly. A redundant takeoff command from the trajectory management software froze the UAV in a hover near ground in flight I2_1.

(B1_2) traversed the corona source and recorded a single peak in UV intensity in front of the corona generator.

Table 1. UAV flights and Datatypes

Tower Base Corona Measurement Flights								
Date	Location	Flight	Description	UV Plot	UV Image	Visible Image	UTM Path	UTM boundary
Tuesday, Nov 15	Tower Base	B1_1	1 st Manual	✓				
	Tower Base	B1_2	1 st Autonomous	✓				
Conductor Height Corona Measurement Flights								
Date	Location	Flight	Description	UV Plot	UV Image	Visible Image	UTM Path	UTM boundary
Tuesday, Nov 15	Tower	T1_2	2 nd Manual	✓				
	Tower	T1_3	3 rd Manual	✓				
Wednesday, Nov 16	Tower	T2_2	2 nd Autonomous	✓		✓	✓	
	Tower	T2_3	3 rd Autonomous	✓	✓	✓	✓	
Autonomous Trajectory Correction Flights								
Date	Location	Flight	Description	UV Plot	UV Image	Visible Image	UTM Path	UTM boundary
Wednesday, Nov 16	Tower Base	I2_2	2 nd ICAROUS			✓	✓	✓
	Tower Base	I2_3	3 rd ICAROUS			✓	✓	✓

Conductor height corona measurement flights ('T flights')

For conductor height flights, the corona generator was attached to the cross-arm of the tower using a bucket truck. A manual flight with multiple traversals of the UV source at increasing altitudes (T1_2 in Table 3) showed that sensors, control and telemetry were working as expected. To frame the UAV in the viewport of the ground-based corona camera, another manual flight (T1_3) was executed without recording from the onboard UV sensors.

Using altitudes and waypoints ascertained from these manual flights, two autonomous flights were conducted at different altitudes with flight paths that traversed the corona source and recorded UV intensity. The weak UV signal at a 16 meter altitude (T2_2) showed two peaks: one from the east-to-west forward flight, and one from the west-to-east return flight⁵. At an 18 meter altitude (flight T2_3), a strong signal was recorded in both the forward and return segments of the flight.

UTM Path records were collected and forwarded to the NASA UTM server for the autonomous flights T2_2 and T2_3, and a ground-based corona camera validated the corona emissions in flight T2_3 at a position corresponding to the peak sensor signal during the forward flight (Table 4). The corona camera overlays red blobs on the visible image at the location of ultraviolet photon emission (left image of Table 4).

⁵ The return flight was fortuitous; the western waypoint happened to extend beyond the autopilot's geofence radius, triggering a 'return to launch' operation. Only the forward flight segment is shown in Table 3 to avoid clutter, but the return segment may be seen in the UTM Path imagery of Table 4.

Table 2. Tower Base Corona Measurement Flights.

©Map data: Google & DigitalGlobe

Flight	Description	UV Plot	Flight Path (front view)	Flight Path (top view)
B1_1	1 st manual			
B1_2	1 st auton.			

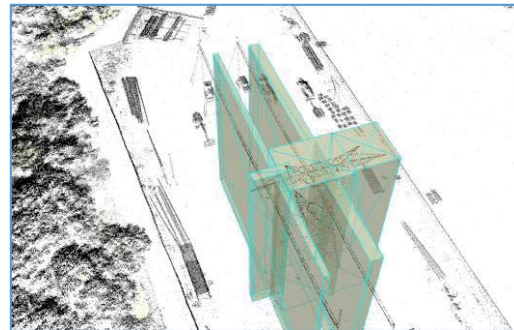
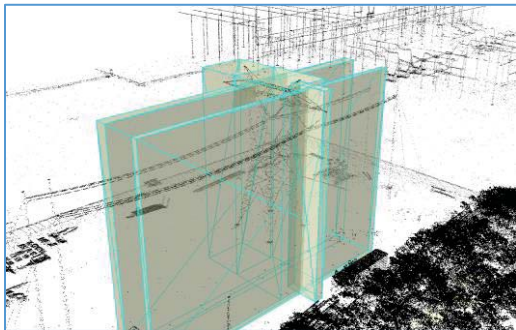


Figure 4. Lidar-derived 2.5D polyhedra for path planning. A set of computed polyhedra (grey rectangles) surrounds the 500kV tower and conductors in these ArcScene views from the southwest (left) and southeast (right). ©Lidar data: Southern Company

Lidar-to-polyhedra geofence preparation

The Autopilot and UTM Flight Path imagery for flights T2_2 and T2_3 include a rectangular enclosure around the tower and conductors composed of polyhedra derived from Southern Company lidar of the Klondike training center. Figure 4 illustrates the polyhedra which were computed via the following 2.5D recipe:

1. The Southern Company lidar in *LAS* format was imported with the spatial projection "NAD 1983 StatePlane Georgia West FIPS 1002 (US Feet)"
2. The ArcGIS function *LASToMultipoint_3d* [22] was used to convert to raster
3. The ArcGIS function *FeatureClassZtoASCII_3d* [22] was used to convert the raster lidar points to (x,y,z) triplets and to export them to a text file.
4. A NASA C++ program
 - a) read the 3D data from the text file,
 - b) converted the coordinates to latitude/longitude/altitude triplets
 - c) traversed the set of triplets, first along lines of latitude and then along lines of longitude, finding the maximum altitude. The effective grid spacing (minimum

- feature spacing) is five decimal places in a decimal latitude and decimal longitude (approximately 0.1 meters of precision at this latitude). A polyhedron from the maximum altitude to ground at that grid location was constructed.
- d) wrote the polyhedron to a KML file for visualization in a 3D map

These polyhedra were used to verify a safe standoff distance from the tower and conductor. In particular, the waypoints for autonomous flights T2_2 and T2_3 were checked to ensure a safe distance from the lidar-derived 2.5D polyhedral “wrapper” around the 500kV tower and conductors.

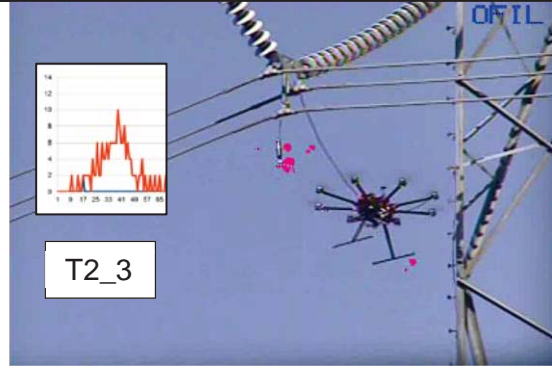
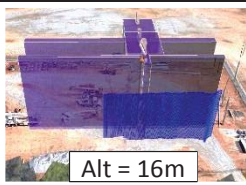

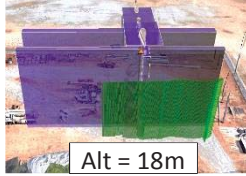

Table 3. Conductor Height Corona Measurement Flights.

© Lidar data: Southern Company; Map data: Google & DigitalGlobe

Flight	Description	UV Sensor	Flight Path (front view)	Flight Path (top view)
T1_2	2 nd manual			
T1_3	3 rd manual	-		
T2_2	2 nd auton.			
T2_3	3 rd auton.		<div style="border: 1px solid black; padding: 5px; margin-top: 10px;"> <p>T2_2 (blue): Alt = 16m</p> <p>T2_3 (green): Alt = 18m</p> </div>	

Table 4. Corona camera verification of compact sensor (left), autopilot flight path tracking (center), and NASA UTM flight path tracking in North American air space (right). The corona camera overlays red blobs on the visible image at the location of ultraviolet photon emission.

© Lidar data: Southern Company; Map data: Google & DigitalGlobe

Flight	Sensor Suite	Autopilot Flight Path	UTM Flight Path
T2_2			
T2_3			

Autonomous trajectory correction flights ('I flights')

The final set of flights (Figure 5) tested ICAROUS [6], which is a trajectory management software technology that monitors the UAV position and corrects the trajectory to keep it within a flight corridor during autonomous waypoint-based flight. Running on an onboard 1 GHz, 8 core microcomputer, ICAROUS reads the telemetry stream that the autopilot sends to the ground station and injects commands into the telemetry stream that the ground station sends to the autopilot. ICAROUS has several capabilities, including detect and avoid [4], geofence conformance [7], dynamic planning [5], stand-off distance monitoring, and return to mission. In this test its return-to-mission capability was exercised in a control flight without wind gust perturbation and in an experimental flight with a transient lateral perturbation that models a wind gust.

The right image of Figure 2 shows the waypoint locations (stars) and camera location (diamond) in the lidar representation of the Klondike test site. In control flight I2_2 (blue traces of Figure 5) the UAV followed a dog-leg path defined by four waypoints near the 500kV tower at five meter altitude. In experimental flight I2_3 (green traces of Figure 5) the UAV was launched along the same path, but the pilot manually perturbed the flight, yanking it to the left to emulate a wind gust. ICAROUS sensed the perturbation, yawed the aircraft back toward the centerline of the preplanned flight path, and 'drove' the UAV back to the intended path. Once the UAV was in conformance with the original flight path, the ICAROUS onboard autonomy yawed the aircraft to face the originally intended nose direction and ceased injecting commands into the autopilot-bound telemetry. The native Pixhawk autopilot waypoint-based navigation capability took over from that time point and completed the flight. This flight was tracked in the national airspace, and the flight paths and boundaries that were stored on the UTM server are shown in the center and right images of Figure 5. The composite image of Figure 6, constructed from three key frames of the video record, illustrates the perturbation and autonomous recovery.

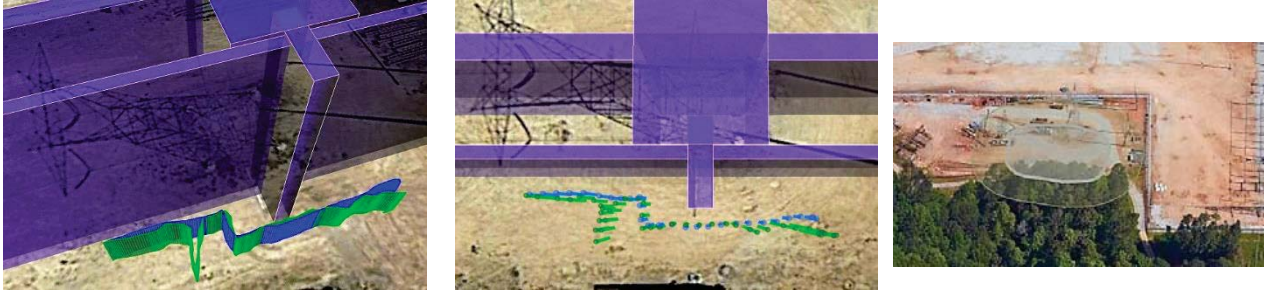


Figure 5. Autonomous trajectory correction flights. Control flight I2_2, blue traces; path perturbation flight I2_3, green traces. Left: autopilot flight paths plotted; center: UTM flight paths; right: UTM boundary for both flights. ©Lidar data: Southern Company; Map data: Google, DigitalGlobe & NASA

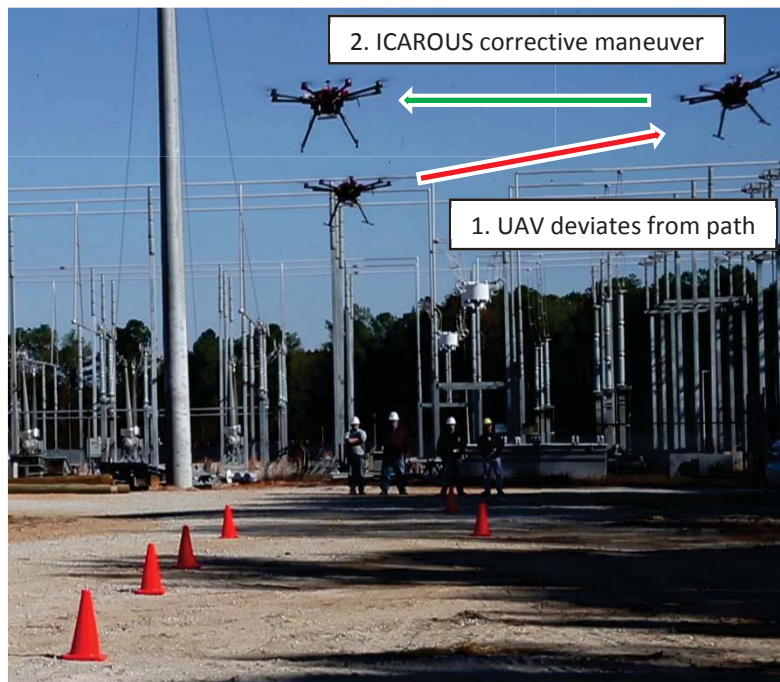


Figure 6. Composite image (overlay video frames) of UAV position at three times during flight I_3. The onboard ICAROUS trajectory management software detected that the UAV was not positioned in the planned flight corridor and maneuvered it to return to the centerline of the flight path.

Data Preparation for Collision Avoidance Using Lidar-derived Polyhedra

For brevity, the term sGPS indicates standalone (single-ended) GPS and the term dGPS indicates differential GPS [15] in this report. The term unipath indicates 'free of multipath interference' [26].

In the flights described above, the polyhedral representation of the 500kV Klondike tower and conductors, derived from Southern Company lidar (Figure 4), was used to verify path planning and to visualize results. While ICAROUS is capable of using an obstacle field represented in this way to enforce a safe UAV trajectory, the poor reliability of GPS near ground structures led us to adopt sGPS and an obstacle standoff distance (six meters, i.e., twenty feet) much greater than the unipath sGPS uncertainty envelope. As a result, the UAV did not fly near enough to ground obstacles during autonomous (waypoint-based) flight to necessitate obstacle avoidance autonomy. That is, ICAROUS was not used to enforce standoff distance from ground obstacles in the 'B' and 'T' flights.

Nevertheless, preparation for this mode of operation is warranted. The 'I' flights demonstrate its feasibility. Techniques that determine the position of a UAV (latitude, longitude and altitude) more precisely and resiliently than sGPS at low altitudes near ground structures are rapidly developing. Position determination via radio [19], image processing (e.g., stereo ranging, triangulation from image recognition of nearby features) and on-the-fly lidar sensing of known structures [17] have the potential to meet or exceed sGPS positioning accuracy near ground structures.

The ability of available onboard autonomy to ingest and process derived polyhedra was tested with the rich lidar map of the Klondike test site. Two polyhedra obstacle fields were prepared from two areas on the site: the first area, 30m x 60m in size, contains the 500kV structure and the second area, 300m x 300m in size, contains buildings, trees and high-voltage bus bars. These areas are labeled '500kV Section' and 'North Quarter,' respectively, in Figure 7 and Table 5. After removing ground lidar points, obstacle maps of the two areas were produced using the 2.5D method described above. In addition, 3D obstacle maps were computed via the following C++ recipe:

1. Convert the (x,y,z) triplets file to a Point Cloud Library [20] PCD file
2. Cluster triplets using cylindrical modeling
 - a. Read point cloud from PCD file
 - b. Find neighborhood groupings using a 1m nearest neighbor radius search, an eigenvector-aligned cylindrical search with 0.4m radius, and an eigenvector difference in angle comparison looking for a difference less than ~26 degrees for the eigenvectors of the largest eigenvalues
 - c. Merge neighborhoods using proximity based metrics
 - d. Assign each neighborhood a label and output them as a labeled point cloud PCD file
3. Compute a minimum bounding box for each of the labeled neighborhoods and output them as a text file
4. Convert the text file of boxes to KML for visualization in a 3D map

Figure 7 shows the computed 2.5D polyhedra at left and the computed 3D polyhedra at right for both areas; Table 5 shows the input point count and the resulting polyhedra count for both areas and methods. The 3D method reduces the data volume approximately by a factor of 50-100, while the 2.5D method reduces the data volume by a factor of 1000-5000. Each input lidar points is a x,y,z triplet. Each output polyhedron is a right rectangular prism with 8 vertices, representable as 8 x,y,z triplets, or more compactly as 3 x,y,z triplets and a height. The numerical data reduction is therefore a factor 3.3-8 lower than the data volume reduction, depending on downstream processing numerical representation.

Input capacity and processing capacity of the version of ICAROUS used in the 'I flights' was tested using the 2.5D polyhedra on the same hardware (1 GHz 8-core microcomputer) used in the flights. It loaded both the 500kV Section and North Quarter maps successfully; its input capacity exceeds 406 polyhedra. To gauge processing capacity, polyhedra from the North Quarter map were added ten at a time until 50% of the processing time was needed for polygon

processing, leaving a 50% compute margin for trajectory calculation, at a trajectory correction rate of once per second. This threshold was observed for ~ 200 polyhedra, corresponding to an area of size 150m x 130m. This result indicates that the obstacle field created from the 500kV Section with the more detailed 3D method (top right in Figure 7) will not impose a processing load too burdensome for real-time 3D obstacle avoidance. However, the obstacle field created from the North Quarter with the 3D method (bottom right in Figure 7), with its many polygonal facets bounding the tree canopy on the Klondike site is not simplified enough for real-time obstacle avoidance. A foliage digital elevation map [21] representation of the tree canopy should bring the geometry count of the North Quarter down to a level that ICAROUS can respond to rapidly.

Several caveats should be made about interpreting the processing capacity test using this data set. First, the geometric processing load is highly dependent on the density and spatial configuration of the polyhedra. Second, as well as simplifying altitude, the 2.5D method computed only aligned orthogonal polyhedra faces oriented east-west and north-south, with obstacles in the east-west direction (the left-right direction in the bottom left of Figure 7) clumped together into a large polyhedron. Third, optimization of ICAROUS is under active development, and it can run on more powerful compact hardware than the microcomputer used in these flights.



Figure 7. Variations of obstacle field size and detail to test ICAROUS capacity. Top left: 500 kV Section, 2.5 D representation. Top right: 500 kV Section, 3D representation. Bottom left: North Quarter, 2.5 D representation. Bottom right: North Quarter, 3D representation. © Lidar data: Southern Company; Map data: Google & DigitalGlobe

Table 5. Data reduction of two areas using 2.5D and 3D algorithms

	Point count (original lidar)	Polyhedra count (2.5D z clustering)	Polyhedra count (3D cylindrical clustering)
500 kV Section	7,965	6	146
North Quarter	2,388,823	406	22,380

A mix of 2.5D and 3D polyhedra representations may be the most suitable way to trade off spatial detail and data volume in mapping the obstacle environment. For example, Figure 8 shows the UV signal during flights T2_2 and T2_3 proximate to a 3D representation of the inspection target, with the North Quarter obstacle represented in 2.5D in the background. The distant North Quarter obstacle do not require full 3D treatment, but a 3D rendition of the 500 kV tower makes it easier to pinpoint the location of a corona fault test signal (red star) and more faithfully outlines the nearby obstacle field for processing with onboard autonomy.

In concert with the 3D tower rendering, sensor results that indicate signal strength and direction help to make the inspection result intuitive. In Figure 8, a green-to-red color scale indicates the magnitude at points along the flight path of the relative UV intensity plotted in Table 3 and Table 4. Visualization of the sensor pose in Figure 8 is provided by direction lines drawn at each sensor measurement point, which extend in the starboard direction from the right

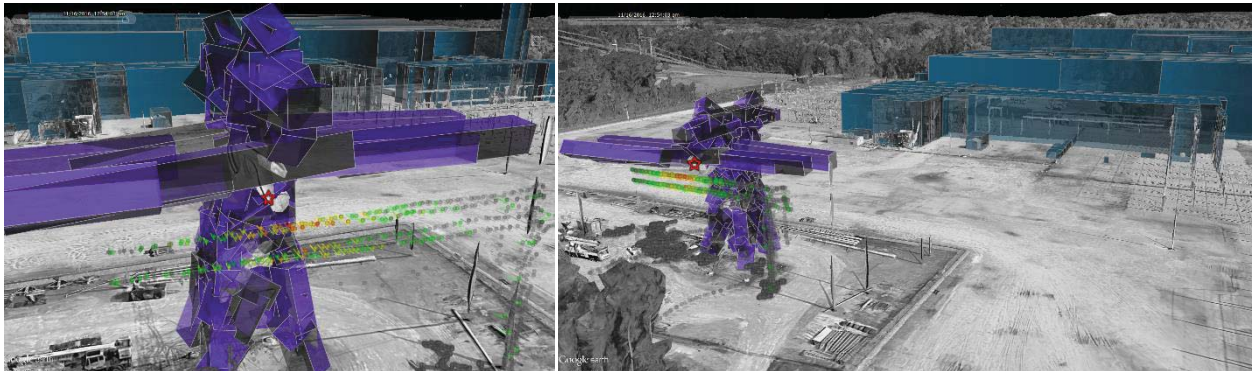


Figure 8. Mixed polyhedra representation for infrastructure inspection. Left image: near view from south-southwest. Right image: far view from far southeast. The 500 kV Section is rendered with the 3D method (foreground, purple) and the North Quarter, of less immediate concern as an obstacle, is rendered with the 2.5D method (background, blue). The corona generator position is indicated by the red star. The UV time series measurements from flights T2_2 (lower trace, 16m altitude) and T2_3 (upper trace, 18m altitude) are shown as a percentage of sensor range with a graduated color scale: dark gray dots indicate that no signal was detected (0% of sensor range), and the scale proceeds through green, yellow, and orange, to red at approximately 75% of sensor range. Colored lines at each measurement point indicate the sensor orientation, correcting for UAV pitch, yaw and roll angles. © Lidar data: Southern Company; Map data: Google & DigitalGlobe

sensor position on the aircraft (Figure 3). To remove artifacts that arise from aircraft attitude, the direction lines are corrected for UAV pitch, yaw, and roll angle. With a point emitter tip, the corona generator radiates isotropically with a $1/R^2$ drop-off in areal flux density. The flight paths approximate chords of a circular planar section of the radiated photon field, with the T2_3 chord (upper trace, 18m altitude) closer to the center of the planar section and to the origin of the spherically symmetric flux field than T2_2 chord (lower trace, 16m altitude). As expected from the optical geometry of Figure 8, the observed signal strength and duration are greater in the T2_3 flight than in the T2_2 flight.

Discussion

Motivation for Lidar-to-Polyhedra Preprocessing

In this study, a preprocessing approach was employed to simplify a rich, precise (sub-decimeter) lidar map to a small number of polyhedra suitable for subsecond processing by ICAROUS on an onboard 1GHz, 8-core microcomputer. A preprocessing approach was necessary because of current limitations in determining the UAV position and the obstacle field boundaries, as discussed in this section.

Secondary reflection and UAV positioning instability

Small UAVs are increasingly available for inspection of and transit near ground structures. However, the ability to determine the spatial position of the UAV accurately (say, within a decimeter) near ground structures remains a challenge. The most commonly used UAV position determination method, single-ended GPS, senses orbital GPS satellite signals with a single antenna mounted on the UAV. At altitudes far above ground structures, sGPS has a unipath positional uncertainty of ± 2 meters horizontally and ± 3 meters vertically with 95% confidence [14]. By comparing the signal received on the UAV antenna with a signal received at an additional antenna mounted at a fixed, surveyed position, a differential GPS measurement can be computed with a much smaller positional uncertainty (± 4 cm or better horizontally and vertically). Transmission of the signal between the two dGPS antenna sites is accomplished via a cable (if both sites are on the ground) or radio link (if one of the sites is airborne).

If the UAV is positioned at low altitude (e.g., below treetops and/or rooftops), its GPS antenna may receive satellite signals along more than one path: a direct (line of sight) path from the satellites and one or more non-direct paths reflected from the terrain and ground structures (i.e., multipath signals). Current sGPS processing methods can reject a second signal that arises from flat terrain reflection. However, methods to disambiguate complex multipath signals from nonplanar terrain and/or ground structures are not yet mature [see for example reference 16]. If not rejected, extraneous reflected (multipath) orbital signals can cause errors that are interpreted as a position shift [16, 23, 24]. In our experience, sGPS position shifts equal to or higher than the 95% confidence unipath horizontal uncertainty (~ 2 meters) are not uncommon at low altitude near vegetation and structures.

Differential measurements do not necessarily improve matters in a multipath environment, since the radio link between GPS receiver units in an air-ground dGPS system is also subject to multipath degradation, which leads to loss of differential lock and the enhanced location precision it provides. The radio signal between GPS receiver units may traverse non-direct paths reflected from the terrain and ground structures, etc.; disambiguating direct from non-direct inter-GPS signals is not mature. Multiple attempts prior to the flights at the Klondike test field to achieve stable, precise UAV position near ground structures via dGPS were not successful [8].

Low altitude vs. high altitude lidar

Ideally, mapping of terrain and structures could be conducted with low altitude lidar-equipped UAVs (see reference [17] for a description of one such mission and a review of algorithmic methods of power line reconstruction from lidar). The cost of equipment and operations would be substantially lower for low altitude UAVs as compared to orbital or high altitude atmospheric (fixed wing or helicopter) platforms, but currently there is not a reliable position determination technology sufficient to geolocate low altitude UAVs with the precision required for sub-decimeter lidar mapping. Precise, stable IMUs (inertial measurement units, e.g., gyroscopes) are too heavy, bulky, and power-hungry for mounting on most low-cost, low

altitude UAVs. Unipath single-ended GPS has a positional uncertainty of 2-3 meters, and both sGPS and dGPS equipment is subject to drop outs, instabilities and high positional inaccuracy when flown near ground structures, as discussed above.

High altitude (e.g., greater than 122 meters, i.e., 400 feet) airborne lidar has been available for decades, and is used to map variations in terrain elevation and the locations and elevations of ground structures, such as trees and buildings, to within a decimeter. Airborne platforms that are equipped with mapping lidar, such as airplanes, helicopters, and satellites are also equipped with instruments to accurately determine the spatial position of the platform, such as high precision IMUs, or high precision differential GPS. IMUs are not dependent on radiolocation, and so are immune to electromagnetic scattering. At high altitudes, differential GPS receivers are far away from electromagnetically scattering structures on the ground, so that the GPS signal used to determine the position of the measurement aircraft is stable and accurate across several overflights (sweeps) of a particular point on earth. Commonly, multiple lidar sweeps are performed over the area to be mapped and the sweeps are conducted from multiple directions, so that no shadowing artifacts degrade the three dimensional lidar point map of the terrain and ground structures [13].

Data volume and processing throughput for high resolution lidar

Due to their high data volume, high fidelity lidar point clouds of terrain and structures are not suitable for a compact representation of an obstacle field. For example, a contemporary high fidelity lidar point cloud with 4 cm horizontal resolution and precision of $\frac{1}{2}$ meter contains tens of millions of individual lidar points in each square mile of ground area (after points along the ground are removed).

Collision avoidance methods suitable for execution in real time on small UAVs, such as the ICAROUS method demonstrated in these flights, are capable of reading the position and velocity of the UAV and calculating a spatial envelope around the UAV that must be obstacle-free to avoid collision with the obstacles. However, given current computer hardware, these collision avoidance software programs are limited in the amount of data they can process to determine obstacle location rapidly (in one second or less). Geometric simplification of the boundaries of obstacle surfaces is required for sufficiently rapid (one second or less) processing by contemporary collision avoidance methods running on compact airborne hardware.

Simplified boundary representations of ground structures have been available for some years [13, 10, 9]. Commonly referred to as digital elevation maps, these representations are used, for example, to map tree canopies in environmental and geological studies [21]. Except for indoor areas and limited outdoor areas, simplified geometric representations of obstacle boundaries derived from lidar point clouds have not been widely used for UAV collision avoidance.

Lidar sensors mounted on the UAV are not suitable for acquiring the lidar the point cloud used to determine obstacle boundaries for two reasons. First, an accurate spatial registration of the point cloud requires accurate spatial determination of the UAV position, and, as described previously, electromagnetic scattering by the obstacles themselves prevents precise determination of the UAV position. Secondly, current compact, low-power lidar sensor/processor payloads are too slow to map out obstacles in a way that is suitable for obstacle avoidance in real time. The time lag in current compact lidar systems between the time of the sensor activation (i.e., emission of a photon burst) and the availability of the resultant processed, geo-referenced lidar point cloud is too high (one or more seconds) for real-time navigation. This time lag arises from a) the sweep time of the 1D laser across the scene and b) the processing and geo-referencing computation time. Just as with lidar data from high altitude airborne acquisition platforms, the raw lidar point cloud of an obstacle field obtained from a low-flying UAV must be preprocessed (ramified to 3D and simplified to a relatively small number geometries) to allow low latency collision avoidance.

Suitability of Lidar-to-Polyhedra Preprocessing for Collision Avoidance

By applying two methods at either side of the range of lidar-to-polyhedra simplification on a real lidar obstacle map, one can approximately bound the degree of data reduction and the corresponding suitability for spatial control of a UAV. The 2.5D method represents the extreme of high data reduction and low spatial fidelity, while the 3D method represents the extreme of lower data reduction and high spatial fidelity. For the two examples selected from the Klondike data set, the 2.5D method provides more than an order of magnitude greater data reduction at the cost of a conservatively outlined obstacle field.

With the higher compression of the 2.5D method, the onboard trajectory management software/hardware required about two seconds to process the North Quarter obstacle field. In the 'I flights' in this study, UAV velocity was 1 m/sec, so that the obstacle collision avoidance during navigation is viable. More powerful computing hardware and dynamic software partitioning of the polyhedra data during the UAV flight is needed if the UAV is a) moving rapidly or b) using a richer representation such as that produced by the 3D method.

Conclusion

This and a previous [8] report document execution of a specific multirotor UAV reference mission, high voltage electrical infrastructure inspection. The reference mission is designed to exercise a realistic air-to-ground integration platform with a UAV sensor payload whose benefit is enabled when airborne and improved with increased navigational precision. By tying sensor result quality to operational and navigational advances, the mission design encouraged broad advances in UAS aviation. The time required to design and package a compact UV sensor for the mission was negligible compared to the time required for UAV platform development and testing; since the only alternative (ground-based UV camera imaging) is over 100 times more costly, the reference mission choice led to an unexpected innovation beneficial to industry.

With this novel onboard sensing capability, test and measurement flights of a UAV were conducted proximate to de-energized high-voltage structures. The previous study focused on UV sensor range and standoff distance; its results and conclusions are confirmed in this study, as the sensor signal was again verified with a ground-based commercial corona camera, and the UAV position was monitored on a local ground station laptop. The flights described in the current report explore two operational and navigational advances: autonomous path correction capability and lidar-to-polyhedron obstacle demarcation. Together, these two sets of flight experiments show that UAV operations for a self-diagnosing power grid can be conducted safely and effectively, and that autonomous technologies can increase the level of safety and effectiveness.

Tracking of the UAV in the national airspace, using the NASA UTM technology, is another key safety aspect of this reference mission. The importance of this tracking was especially salient at Southern Company's Klondike training facility in Lithonia, Georgia, which is 17.5 miles due east of the Hartsfield–Jackson Atlanta International Airport, beneath a busy landing approach corridor. Passenger aircraft on descent approach to KATL flew 5000 feet overhead [25] at a rate of about once per minute; the UTM system tracked the UAV within a heterogeneous airspace during these experiments. Before and during each infrastructure inspection flight, the UTM server verified that there were no aviation safety notifications.

High accuracy, high precision aerial lidar maps are available for most high voltage infrastructure in North America. The raw data volume of those maps is too high for airborne trajectory management at this time, even for the modest areas that may be traversed on a single battery charge by a rotary UAV. Detailed 3D polygon shells were computed that enclose the lidar points, faithfully enough for flight planning and obstacle avoidance, at 30-100 times lower data volume. Even simpler 2.5D processing produced a spatial representation sufficient

for planning and safety, and reduced the data volume by a further factor of 30-100. A set of 2.5D polyhedra that enclosed a 500 kV transmission tower and conductors was used to plan a UAV flight path past the tower and parallel to the conductors. The path was flown twice, with the autopilot listening for instructions from onboard ICAROUS autonomous path conformance technology. In the first flight, the UAV was allowed to follow the path exactly, so that ICAROUS did not need to issue course corrections. In the second flight, the UAV was veered off-course as if struck by a side wind gust. ICAROUS issued course corrections to bring the aircraft back to the center of the flight path; once the UAV was returned to a safe trajectory, the autopilot resumed the flight to completion.

In conclusion, the goals of the high voltage infrastructure inspection reference mission design were met -- UAV navigation technology was advanced while accomplishing a task with economic and societal benefit. Compelling UAV operational and detection methods were developed, airspace awareness (via UTM) was exercised in a busy flight corridor, newly implemented path management autonomy was deployed onboard to assure flight safety in an intrinsically valuable application, and creation of compact spatial geofences for UAV navigation from highly accurate industry lidar mapping data was driven from conception to flight readiness. The multiple, complementary aviation advances demonstrated in conjunction with advances specific to transmission line inspection show progress toward a self-diagnosing power grid.

References

1. Matikainen, Leena, et al. "Remote sensing methods for power line corridor surveys." *ISPRS Journal of Photogrammetry and Remote Sensing* 119 (2016): 10-31.
2. Menendez, Oswaldo A., Marcelo Perez, and Fernando A. Auat Cheein. "Vision based inspection of transmission lines using unmanned aerial vehicles." *Multisensor Fusion and Integration for Intelligent Systems (MFI), 2016 IEEE International Conference on*. IEEE, 2016.
3. Prevot, Thomas, et al. "UAS traffic management (UTM) concept of operations to safely enable low altitude flight operations." 16th AIAA Aviation Technology, Integration, and Operations Conference. 2016.
4. Muñoz, César, et al. "DAIDALUS: detect and avoid alerting logic for unmanned systems." Digital Avionics Systems Conference (DASC), 2015 IEEE/AIAA 34th. IEEE, 2015.
5. Balachandran, Swee, et al. "A Path Planning Algorithm to Enable Well-Clear Low Altitude UAS Operation Beyond Visual Line of Sight." Twelfth USA/Europe Air Traffic Management Research and Development Seminar (ATM2017).
6. Consiglio, María, et al. "ICAROUS: Integrated configurable algorithms for reliable operations of unmanned systems." Digital Avionics Systems Conference (DASC), 2016 IEEE/AIAA 35th. IEEE, 2016.
7. Narkawicz, Anthony, and George Hagen. "Algorithms for collision detection between a point and a moving polygon, with applications to aircraft weather avoidance." Proceedings of the AIAA Aviation Conference. 2016.
8. Moore, Andrew J., Matthew Schubert, and Nicholas Rymer. "Autonomous Inspection of Electrical Transmission Structures with Airborne UV Sensors-NASA Report on Dominion Virginia Power Flights of November 2016." NASA Technical Memo 2017-219611 (2017).
9. Chida, Akisato, and Hiroshi Masuda. "Reconstruction of polygonal prisms from point-clouds of engineering facilities." *Journal of Computational Design and Engineering* 3.4 (2016): 322-329.
10. Kwon, Soon-Wook, et al. "Fitting range data to primitives for rapid local 3D modeling using sparse range point clouds." *Automation in construction* 13.1 (2004): 67-81.

11. Mizoguchi, Tomohiro, et al. "Manhattan-world assumption for as-built modeling industrial plant." *Key Engineering Materials*. Vol. 523. Trans Tech Publications, 2012.
12. Pendleton, Scott Drew, et al. "Perception, Planning, Control, and Coordination for Autonomous Vehicles." *Machines* 5.1 (2017): 6.
13. Vosselman, George, et al. "Recognising structure in laser scanner point clouds." *International archives of photogrammetry, remote sensing and spatial information sciences* 46.8 (2004): 33-38.
14. Civil Report Card On GPS Performance Nov 2016. (2016, December). Retrieved March 15, 2017, from http://www.nstb.tc.faa.gov/reports/ReportCards/2016_11.pdf
15. Parkinson, Bradford W., and Per K. Enge. "Differential gps." *Global Positioning System: Theory and applications*. 2 (1996): 3-50.
16. Sokhandan, Negin. "A Novel Multipath Estimation and Tracking Algorithm for Urban GNSS Navigation Applications." *Proceedings of ION GNSS 2013* (2013): 16-20.
17. Ippolito, Corey, Kalmanje Krishnakumar, and Sebastian Hening. "Preliminary results of powerline reconstruction from airborne LiDAR for safe autonomous low-altitude urban operations of small UAS." *SENSORS, 2016 IEEE*. IEEE, 2016.
18. Wolf, Gene. "LiDAR Meets NERC Alert." *Transmission & Distribution World* 63.8 (2011): 9-13.
19. Pérez-Grau, F. J., et al. "Long-term aerial robot localization based on visual odometry and radio-based ranging." *Unmanned Aircraft Systems (ICUAS), 2016 International Conference on*. IEEE, 2016.
20. Rusu, Radu Bogdan, and Steve Cousins. "3d is here: Point cloud library (pcl)." *Robotics and automation (ICRA), 2011 IEEE International Conference on*. IEEE, 2011.
21. Lefsky, Michael A., et al. "Lidar remote sensing for ecosystem studies: Lidar, an emerging remote sensing technology that directly measures the three-dimensional distribution of plant canopies, can accurately estimate vegetation structural attributes and should be of particular interest to forest, landscape, and global ecologists." *AIBS Bulletin* 52.1 (2002): 19-30.
22. ESRI 2016. *ArcGIS Desktop: Release 10.4.1*. Redlands, CA: Environmental Systems Research Institute.
23. Weill, Lawrence R. "Conquering mutlipath: The GPS accuracy battle." *GPS world* 4 (1997): 59-66.
24. Xie, Peng, and M. G. Petovello. "Improving high sensitivity GNSS receiver performance in multipath environments for vehicular applications." In *Proc. ION/GNSS*. 2013.
25. "ILS RWY 26R HARTSFIELD-JACKSON ATLANTA INTL (ATL)," Federal Aviation Administration, September 2014, http://aeronav.faa.gov/d-tpp/1708/00026126RSAC1_2.PDF [retrieved 16 Aug. 2017].
26. Serrano, Luis, Don Kim, and Richard B. Langley. "Carrier-phase multipath calibration in GPS-RTK machine-guidance applications." In *Position, Location and Navigation Symposium, 2008 IEEE/ION*, pp. 479-488. IEEE, 2008.

Appendix 1. Inventory of Flights

Tower Base Corona Measurement Flights							
Date	Location	Flight	Description	UV Plot	UV Image	Visible Image	UTM path
Tuesday, Nov 15	Tower Base	B1_1	1 st Manual	✓			
	Tower Base	B1_2	1 st Autonomous	✓			
Conductor Height Corona Measurement Flights							
Date	Location	Flight	Description	UV Plot	UV Image	Visible Image	UTM path
Tuesday, Nov 15	Tower	T1_1	1 st Manual				
	Tower	T1_2	2 nd Manual	✓			
	Tower	T1_3	3 rd Manual	✓			
Wednesday, Nov 16	Tower	T2_1	1 st Autonomous, aborted			✓	✓
	Tower	T2_2	2 nd Autonomous	✓		✓	✓
	Tower	T2_3	3 rd Autonomous	✓	✓	✓	✓
Autonomous Trajectory Correction Flights							
Date	Location	Flight	Description	UV Plot	UV Image	Visible Image	UTM path
Wednesday, Nov 16	Tower Base	I1_1	1 st ICAROUS, aborted			✓	✓
	Tower Base	I1_2	2 nd ICAROUS			✓	✓
	Tower Base	I1_3	3 rd ICAROUS			✓	✓

Appendix 2. Experimental Equipment

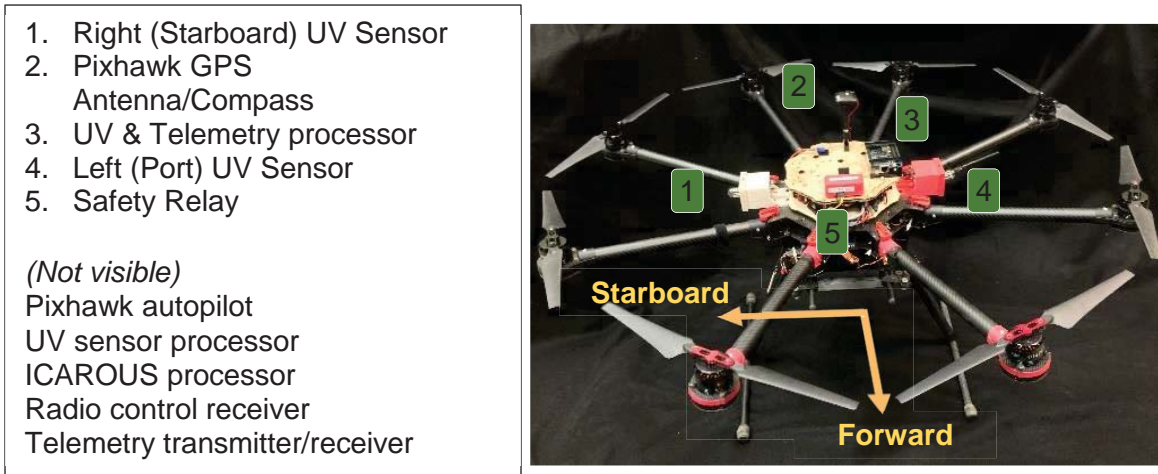


Figure 9. The aircraft FA3WEANXWH was used in all flights. It is comprised of a DJI S1000 frame, a Pixhawk autopilot, three onboard single-board computers, and custom sensing and telemetry electronics.

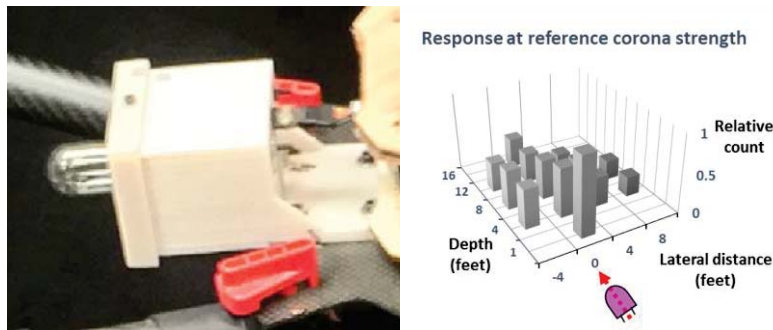


Figure 10. Left: The Hamamatsu R13192, which can sense a 100 kV corona at a distance of ~ 3.6 meters (12 feet). Center: Sensitivity plot of R13192.

The Electro-Technic Products BD-20A High Frequency Generator was used to produce corona in these experiments. The following were used for image capture and computing: UVolle-VC corona camera, Canon EOS 1D Mark II visible camera, Dell Precision M6700 laptop (running Centos Linux), Panasonic CF-54 Toughbook (running Windows 8). The following were used for communications and control: Spektrum 18 channel transmitter, 3DR 915 MHz telemetry link, Verizon Jetpack LTE/Wifi hotspot.

Component	Software	Version
Pixhawk autopilot	Arducopter	3.3.3
Ground station Dell laptop	Centos Linux	6.8
Ground control (operation)	APMPlanner	2.0.19-rc4
Ground control (configuration)	QGroundcontrol	StableV3.0
Telemetry monitor	MavProxy	1.4.42
Power distribution voltage control	Castle Link CC BEC Pro	3.62.00

Source	Frequency	Purpose
3DR Radio	915MHz (Ch. 1)	Ground station command and control
Spektrum	2.4GHz	R/C command and control

Figure 11. Software package versions (top) and radio frequencies (bottom) used in the flights

Table 6. Custom mission software

Custom Software	Functionality	Substrate	Origin
Commbox	On-board: gather UV sensor data and convert into Arducopter/Mavlink telemetry protocol, forward commands to autopilot, and forward telemetry to ground station. On ground station: receive UV and other telemetry, and log UV data to separate file.	Onboard 1GHz, 8-core microcomputer	NASA Langley A2I group
UV_Pulse	On-board: read from each UV sensor, encode pulse count and send to Commbox	Onboard microcontroller	NASA Langley A2I group
UTM client	Ground-to-server: gather UAV location estimate from groundstation telemetry and post to UTM server	Panasonic Toughbook	NASA Ames UTM group
RelAlt	Postprocessing: script to substitute relative altitude (instead of absolute altitude) before export from telemetry log to KML, for rendering in Google Earth	Any	NASA Langley A2I group
ICAROUS	On-board: compare autopilot location estimate to preplanned flight path and correct trajectory as needed to return to flight path.	Onboard 1GHz, 8-core microcomputer	NASA Langley ICAROUS group
Geofence uploader	Ground-to-air: read geofence and obstacle field polyhedra and send to ICAROUS.	Groundstation Dell	NASA Langley A2I group

REPORT DOCUMENTATION PAGE

Form Approved
OMB No. 0704-0188

The public reporting burden for this collection of information is estimated to average 1 hour per response, including the time for reviewing instructions, searching existing data sources, gathering and maintaining the data needed, and completing and reviewing the collection of information. Send comments regarding this burden estimate or any other aspect of this collection of information, including suggestions for reducing the burden, to Department of Defense, Washington Headquarters Services, Directorate for Information Operations and Reports (0704-0188), 1215 Jefferson Davis Highway, Suite 1204, Arlington, VA 22202-4302. Respondents should be aware that notwithstanding any other provision of law, no person shall be subject to any penalty for failing to comply with a collection of information if it does not display a currently valid OMB control number.
PLEASE DO NOT RETURN YOUR FORM TO THE ABOVE ADDRESS.

1. REPORT DATE (DD-MM-YYYY) 01-10-2017	2. REPORT TYPE Technical Memorandum	3. DATES COVERED (From - To)
--	---	-------------------------------------

4. TITLE AND SUBTITLE UAV Inspection of Electrical Transmission Infrastructure with Path Conformance Autonomy and Lidar-based Geofences NASA Report on UTM Reference Mission Flights at Southern Company Flights November 2016	5a. CONTRACT NUMBER
	5b. GRANT NUMBER
	5c. PROGRAM ELEMENT NUMBER

6. AUTHOR(S) Moore, Andrew J.; Schubert, Matthew; Rymer, Nicholas; Balachandran, Swee; Consiglio, Maria C.; Munoz, Cesar A.; Smith, Joshua; Lewis, Dexter; Schneider, Paul	5d. PROJECT NUMBER
	5e. TASK NUMBER
	5f. WORK UNIT NUMBER 154692.02.70.07.02

7. PERFORMING ORGANIZATION NAME(S) AND ADDRESS(ES) NASA Langley Research Center Hampton, VA 23681-2199	8. PERFORMING ORGANIZATION REPORT NUMBER L-20871
---	--

9. SPONSORING/MONITORING AGENCY NAME(S) AND ADDRESS(ES) National Aeronautics and Space Administration Washington, DC 20546-0001	10. SPONSOR/MONITOR'S ACRONYM(S) NASA
	11. SPONSOR/MONITOR'S REPORT NUMBER(S) NASA-TM-2017-219673

12. DISTRIBUTION/AVAILABILITY STATEMENT

Unclassified
Subject Category 01
Availability: NASA STI Program (757) 864-9658

13. SUPPLEMENTARY NOTES

14. ABSTRACT
Flights at low altitudes in close proximity to electrical transmission infrastructure present serious navigational challenges: GPS and radio communication quality is variable and yet tight position control is needed to measure defects while avoiding collisions with ground structures. To advance unmanned aerial vehicle (UAV) navigation technology while accomplishing a task with economic and societal benefit, a high voltage electrical infrastructure inspection reference mission was designed. An integrated air-ground platform was developed for this mission and tested in two days of experimental flights to determine whether navigational augmentation was needed to successfully conduct a controlled inspection experiment. The airborne component of the platform was a multirotor UAV built from commercial off-the-shelf hardware and software, and the ground component was a commercial laptop running open source software. A compact ultraviolet sensor mounted on the UAV can locate "hot spots" (potential failure points in the electric grid), so long as the UAV flight path adequately samples the airspace near the power grid structures.

15. SUBJECT TERMS

Traffic management technology; UAV; UTM; Unmanned aerial vehicle

16. SECURITY CLASSIFICATION OF:			17. LIMITATION OF ABSTRACT	18. NUMBER OF PAGES	19a. NAME OF RESPONSIBLE PERSON
a. REPORT	b. ABSTRACT	c. THIS PAGE			STI Help Desk (email: help@sti.nasa.gov)
U	U	U	UU	27	19b. TELEPHONE NUMBER (Include area code) (757) 864-9658